European Conference on Computational Fluid Dynamics
ECCOMAS CFD 2006
P. Wesseling, E. Oñate and J. Périaux (Eds)

MODEL REDUCTION BY PROPER ORTHOGONAL DECOMPOSITION FOR LAMBDA-OMEGA SYSTEMS

H. Müller* **and S. Volkwein†**

*University of Graz
Institute for Mathematics and Scientific Computing
Heinrichstraße 36
8010 Graz, Austria
e-mail: hannes.mueller@stud.uni-graz.at

†University of Graz
Institute for Mathematics and Scientific Computing
Heinrichstraße 36
8010 Graz, Austria
e-mail: stefan.volkwein@uni-graz.at
web page: http://www.uni-graz.at/imawww/volkwein/

Key words: Model reduction, proper orthogonal decomposition, reaction-diffusion systems, lambda-omega systems, chemical turbulence.

Abstract. *Proper orthogonal decomposition (POD) is a powerful technique for model reduction of linear and non-linear systems. It is based on a Galerkin type discretization with basis elements created from the system itself. In this work POD is used to derive low-order models for a so-called lambda-omega (λ-ω) system that is a universal model to investigate two-species reaction-diffusion problems. In the case of fast reaction kinetics and small diffusion, these systems evolve to turbulent behavior. The performance of the POD model reduction is studied in dependence on the parameters of the λ-ω system. With increasing turbulence more POD modes are needed to capture the dynamics of the full system in a satisfactory way.*

1 INTRODUCTION

Reaction diffusion systems describe processes that can be often found in nature. In particular, lambda-omega (λ-ω) systems can be used to study two species reaction diffusion systems. They are used as a 'universal model' to study chemical reaction processes [19], to describe the dynamics of biological systems [24], to investigate the mechanism of pattern formation [7], and to analyze the occurence of turbulent behavior [23]. In [8] a technical application based on pattern forming systems is considered. Optimal control problems for the λ-ω system are considered in [5, 6].

The amount of computing time and space needed for the solution of such a dynamical system can be very large. Due to the importance of possible applications related to

λ-ω systems we apply a model reduction technique to derive a low-dimensional approximation. Here we utilize proper orthogonal decomposition (POD) that is a method to derive reduced-order models for systems of differential equations. It is based on projecting the system onto subspaces consisting of basis elements that contain characteristics of the expected solution. This is in contrast to, e.g., finite element techniques, where the elements of the subspaces are uncorrelated to the physical properties of the system that they approximate. Dependent on the parameters of the λ-ω system it shows different turbulent behavior. With increasing turbulence more POD modes are needed to capture the dynamics of the full system.

Let us finally briefly comment on further literature containing applications of POD. It is successfully used in different fields including signal analysis and pattern recognition (see, e.g., [10]), fluid dynamics and coherent structures (see, e.g., [12, 28]) and more recently in control theory (see, e.g., [2, 4, 18, 22]) and inverse problems [3]. Surprisingly good approximation properties are reported for POD based schemes in several articles, see [9, 30], for example. The relationship between POD and balancing is considered in [21, 26, 31]. Error analysis for nonlinear dynamical systems in finite dimensions are carried out in [13, 25]. In [16, 17] error estimates for POD Galerkin approximations are derived for non-linear parabolic differential equations. These results are extended to linear-quadratic optimal control problems in [11]. In [14] error estimates for POD Galerkin schemes for linear and certain semi-linear elliptic, parameter dependent systems are proved. Parameter estimation problems for coefficients in elliptic partial differential equations are solved numerically by POD approximations in [15].

The article is organized in the following manner: In Section 2 we introduce the λ-ω system and review some of its properties. The POD method and the reduced-order modeling is desribed in Section 3. Section 4 is devoted to present some numerical experiments including a predictor-corrector method, where we compute the POD solution by splitting the POD modes in lower and higher modes as usual done in non-linear Galerkin projections. In the last section we draw some conclusions.

2 LAMBDA-OMEGA SYSTEMS

Let $\Omega = (0,1) \times (0,1)$ be the spatial domain with Lipschitz-boundary $\Gamma = \partial\Omega$. By $n \in \mathbb{R}^2$ we denote the outward normal vector on Γ. For $T > 0$ we set $Q = (0,T) \times \Omega$ and $\Sigma = (0,T) \times \Omega$. For given diffusion parameter $\sigma > 0$ the functions $u, v : \overline{Q} \to \mathbb{R}$ solve

$$\begin{pmatrix} u_t(t,\mathbf{x}) \\ v_t(t,\mathbf{x}) \end{pmatrix} = \begin{pmatrix} \lambda(s) & -\omega(s) \\ \omega(s) & \lambda(s) \end{pmatrix} \begin{pmatrix} u(t,\mathbf{x}) \\ v(t,\mathbf{x}) \end{pmatrix} + \begin{pmatrix} \sigma\Delta u(t,\mathbf{x}) \\ \sigma\Delta v(t,\mathbf{x}) \end{pmatrix} \quad \text{for all } (t,\mathbf{x}) \in Q, \tag{1a}$$

where $s = u(t,\mathbf{x})^2 + v(t,\mathbf{x})^2$ holds and $\mathbf{x} = (x,y)$. We supply (1a) with homogeneous Dirichlet boundary conditions

$$u(t,\mathbf{s}) = v(t,\mathbf{s}) = 0 \quad \text{for all } (t,\mathbf{s}) \in \Sigma \tag{1b}$$

or homogeneous Neumann boundary conditions

$$\sigma \frac{\partial u}{\partial n}(t, \mathbf{s}) = \sigma \frac{\partial v}{\partial n}(t, \mathbf{s}) = 0 \quad \text{for all } (t, \mathbf{s}) \in \Sigma \tag{1c}$$

and with the initial conditions

$$u(0, \mathbf{x}) = u_\circ(\mathbf{x}) \text{ for all } \mathbf{x} \in \Omega \quad \text{and} \quad v(0, \mathbf{x}) = v_\circ(\mathbf{x}) \text{ for all } \mathbf{x} \in \Omega. \tag{1d}$$

In (1d) the functions $u_\circ$, $v_\circ : \Omega \to \mathbb{R}$ are given. The initial-boundary value problem (1) is called λ-ω system.

To model chemical turbulence the choice

$$\lambda(s) = 1 - s \quad \text{and} \quad \omega(s) = -\beta s \quad \text{with } \beta > 0 \tag{2}$$

is proposed in [20, 24, 27]. Existence of a unique solution pair (u, v) to (1) together with (2) is proved in [5] by using the Leray-Schauder fixed point theorem and the Gronwall lemma.

Remark 1 Note that (1a) together with (2) can be written as

$$z_t(t, \mathbf{x}) = z(t, \mathbf{x}) - \big(1 + \imath\beta\big)|z(t, \mathbf{x})|^2 z(t, \mathbf{x}) + \sigma \Delta z(t, \mathbf{x}) \quad \text{for all } (t, \mathbf{x}) \in Q, \tag{3}$$

where $z = u + \imath v : \Omega \to \mathbb{C}$ with the imaginary unit $\imath = \sqrt{-1}$ holds. Equation (3) is a special form of the complex Ginzburg-Landau model [29], which has been used widely in physics as a generic amplitude equation near the onset of instabilities that lead to turbulent/chaotic behavior in fluid dynamics.

The solution pair (u, v) to (1) has the form of spiral waves that persist indefinitely. In Figure 1 snaphots of the λ-ω system are plotted for the solution u at the time $t = 100$ for homogeneous Dirichlet boundary conditions and in Figure 2 for homogeneous Neumann boundary conditions. The corresponding plots for the solution v are similar to Figure 1 respectively Figure 2. If the parameter β in (2) increases, the spiral waves are not stable anymore and tubulent behavior can be observed.

The goal of our work is to solve (1) by a reduced-order approach utilizing POD. This approach is described in the next section.

3 POD REDUCED-ORDER MODELING

In this section we describe the POD approximation of the λ-ω system. By (u, v) we denote the unique solution pair to (1). We introduce the equidistant time grid $\{t_j\}_{j=1}^n$ by

$$\Delta t = \frac{T}{n-1} \quad \text{and} \quad t_j = (j-1)\Delta t \text{ for } j = 1, \ldots, n. \tag{4}$$

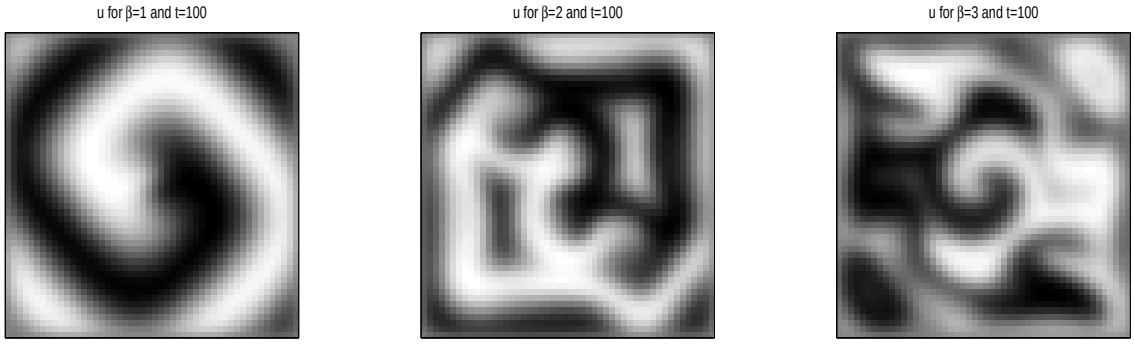

Figure 1: Solution u of the λ-ω system at the time $t = 100$ for homogeneous Dirichlet boundary conditions for $\beta \in \{1, 2, 3\}$ in (2) and for initial conditions $u_\circ(x, y) = (y - 1/2)$, $v_\circ(x, y) = (x - 1/2)/2$.

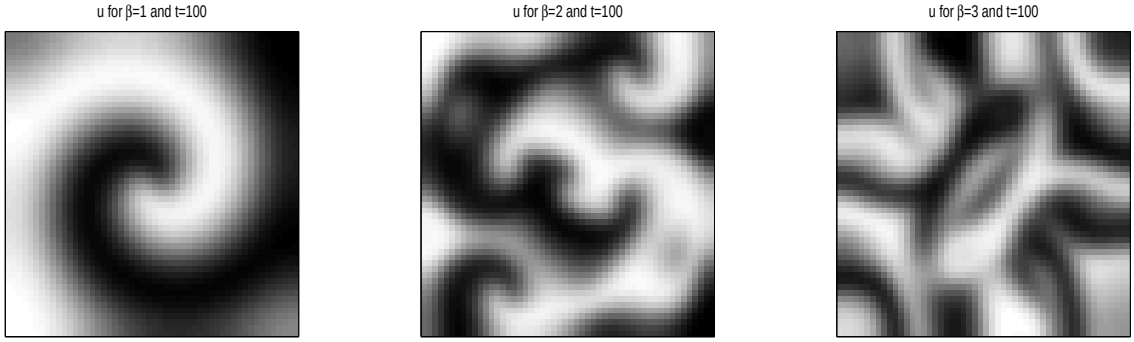

Figure 2: Solution u of the λ-ω system at the time $t = 100$ for homogeneous Neumann boundary conditions and for $\beta \in \{1, 2, 3\}$ in (2) and for initial conditions $u_\circ(x, y) = (y - 1/2)$, $v_\circ(x, y) = (x - 1/2)/2$.

To simplify the presentation we choose an equidistant mesh in (4). Of course, the approach is analogous for non-equidistant time grids; see, e.g., [17]. Let $\bar{u}$, $\bar{v} : \overline{Q} \to \mathbb{R}$ be given offsets. Further, $\{(u_j, v_j)\}_{j=1}^n$ denotes the solution pairs to (1) evaluated at the time grid $\{t_j\}_{j=1}^n$, i.e.,

$$u_j(\mathbf{x}) = u(t_j, \mathbf{x}),\ v_j(\mathbf{x}) = v(t_j, \mathbf{x}) \quad \text{for } j = 1, \ldots, n \text{ and } \mathbf{x} \in \Omega.$$

Remark 2 Common choices for the offsets — in particular in the context of turbulent flows [12] — are mean values, e.g., $(\bar{u}, \bar{v}) = (u_{\text{mean}}, v_{\text{mean}})$, where

$$u_{\text{mean}} = \frac{1}{n} \sum_{j=1}^{n} u_j \quad \text{and} \quad v_{\text{mean}} = \frac{1}{n} \sum_{j=1}^{n} v_j.$$

Since the spatial functions u_j and v_j satisfy either homogeneous Dirichlet or homogeneous Neumann boundary conditions, their mean values possesses the same boundary conditions.

Next we take the snapshots

$$\hat{u}_j = u_j - \bar{u} \quad \text{and} \quad \hat{v}_j = v_j - \bar{v} \quad \text{for } j = 1, \dots, n.$$

Introducing the L^2 inner product

$$\langle \varphi, \psi \rangle = \int_\Omega \varphi \psi \, \mathrm{d}\mathbf{x} \tag{5}$$

and the associated induced norm $\|\varphi\| = \sqrt{\langle \varphi, \varphi \rangle}$ we determine a POD basis of rank $\ell \in \{1, \dots, n\}$ for the function u by solving the constrained minimization problem

$$\min_{\psi_1, \dots, \psi_\ell} \sum_{j=1}^{n} \alpha_j \left\| \hat{u}_j - \sum_{i=1}^{\ell} \langle \hat{u}_j, \psi_i \rangle \, \psi_i \right\|^2 \quad \text{s.t.} \quad \langle \psi_i, \psi_j \rangle = \delta_{ij}, \ 1 \le i, j \le \ell, \tag{$\mathbf{P}_u^\ell$}$$

where the α_j's are chosen as the trapezoidal weights $\alpha_1 = \alpha_n = \Delta t/2$ and $\alpha_j = \Delta t$ for $2 \le j \le n-1$. In ($\mathbf{P}_u^\ell$) we denote by δ_{ij} the Kronecker symbol with $\delta_{ij} = 1$ for $i = j$ and $\delta_{ij} = 0$ otherwise.

Remark 3 Instead of (5) one can also utilize the H^1 inner product

$$\langle \varphi, \psi \rangle_{H^1} = \int_\Omega \varphi \psi + \nabla \varphi \cdot \nabla \psi \, \mathrm{d}\mathbf{x}$$

with its associated induced norm $\| \cdot \|_{H^1}$; see [14, 16, 17].

Analogously, a POD basis of rank $\ell \in \{1, \dots, n\}$ for the function v solves

$$\min_{\phi_1, \dots, \phi_\ell} \sum_{j=1}^{n} \alpha_j \left\| \hat{v}_j - \sum_{i=1}^{\ell} \langle \hat{v}_j, \phi_i \rangle \, \phi_i \right\|^2 \quad \text{s.t.} \quad \langle \phi_i, \phi_j \rangle = \delta_{ij}, \ 1 \le i, j \le \ell. \tag{$\mathbf{P}_v^\ell$}$$

The solutions to ($\mathbf{P}_u^\ell$) and ($\mathbf{P}_v^\ell$) are given by the solution to the symmetric eigenvalue problems [12, 30]

$$\mathcal{R}_u \psi_i = \lambda_i \psi_i \quad \text{and} \quad \mathcal{R}_v \phi_i = \mu_i \phi_i \quad \text{for } i = 1, \dots, \ell, \tag{6}$$

respectively, where

$$\mathcal{R}_u \psi = \sum_{j=1}^{n} \alpha_j \, \langle \hat{u}_j, \psi \rangle \, \hat{u}_j, \qquad \lambda_1 \ge \lambda_2 \ge \ldots \ge \lambda_\ell > 0,$$

$$\mathcal{R}_v \phi = \sum_{j=1}^{n} \alpha_j \, \langle \hat{v}_j, \phi \rangle \, \hat{v}_j, \qquad \mu_1 \ge \mu_2 \ge \ldots \ge \mu_\ell > 0.$$

Remark 4 (Methods of snapshot [28]**)** Let us supply $\mathbb{R}^n$ with the weighted inner product

$$\langle \varphi, \chi \rangle_{\mathbb{R}^n} = \sum_{i=1}^{n} \alpha_i \varphi^i \chi^i \quad \text{for } \varphi = (\varphi^1, \dots, \varphi^n)^T, \chi = (\chi^1, \dots, \chi^n)^T \in \mathbb{R}^n.$$

We define the symmetric non-negative matrix $\mathcal{K}_u \in \mathbb{R}^{n \times n}$ with the elements $\langle \hat{u}_i, \hat{u}_j \rangle$, $1 \le i, j \le n$, and consider the eigenvalue problem

$$\mathcal{K}_u \varphi_i = \lambda_i \varphi_i, \ 1 \le i \le \ell \quad \text{and} \quad \langle \varphi_i, \varphi_j \rangle_{\mathbb{R}^n} = \delta_{ij}, \ 1 \le i, j \le \ell. \tag{7}$$

Often the matrix $\mathcal{K}_u$ is called a correlation matrix for the snapshots ensemble $\{\hat{u}_j\}_{j=1}^n$. From singular value decomposition it follows that $\mathcal{K}_u$ has the same eigenvalues $\{\lambda_i\}_{i=1}^d$ as the operator $\mathcal{R}_u$. Furthermore, the POD basis functions are given by the formula

$$\psi_i = \frac{1}{\sqrt{\lambda_i}} \sum_{j=1}^{n} \alpha_j (\varphi_i)^j \hat{u}_j \quad \text{for } i = 1, \dots, \ell,$$

where $(\varphi_i)^j$ denotes the jth-component of the eigenvector $\varphi_i \in \mathbb{R}^n$. This approach is called *methods of snapshots*. Analogously, the POD basis $\{\phi_i\}_{i=1}^{\ell}$ can be computed by defining the symmetric non-negative matrix $\mathcal{K}_v \in \mathbb{R}^{n \times n}$ with the elements $\langle \hat{v}_i, \hat{v}_j \rangle$, $1 \le i, j \le n$, solving the eigenvalue problem

$$\mathcal{K}_v \chi_i = \mu_i \chi_i, \ 1 \le i \le \ell, \quad \text{and} \quad \langle \chi_i, \chi_j \rangle_{\mathbb{R}^n} = \delta_{ij}, \ 1 \le i, j \le \ell, \tag{8}$$

and setting

$$\phi_i = \frac{1}{\sqrt{\mu_i}} \sum_{j=1}^{n} \alpha_j (\chi_i)^j \hat{v}_j \quad \text{for } i = 1, \dots, \ell.$$

Note that (7) and (8) are eigenvalue problems in $\mathbb{R}^n$, whereas (6) are eigenvalue problems in $L^2(\Omega)$ that have to be discretized for numerical realization. In particular, for two- or three-dimensional domains Ω it turns out that the POD basis should be computed by solving (7) instead the discretized version of (6). In our numerical test examples (see Section 4) we compute the POD basis by utilizing the methods of snapshots.

Remark 5 Note that $(\mathbf{P}_u^{\ell})$ can be interpreted as the trapezoidal approximation of

$$\min_{\psi_1, \dots, \psi_\ell} \int_0^T \left\| (u(t, \cdot) - \bar{u}) - \sum_{i=1}^{\ell} \langle u(t, \cdot) - \bar{u}, \psi_i \rangle \, \psi_i \right\|^2 \mathrm{d}t \quad \text{s.t.} \quad \langle \psi_i, \psi_j \rangle = \delta_{ij}, \ 1 \le i, j \le \ell.$$

This relationship is used in [17] to study asymptotic convergence properties of the eigenfunctions $\{\psi_i\}_{i=1}^{\ell}$ and the corresponding eigenvalues $\{\lambda_i\}_{i=1}^{\ell}$ as the mesh size Δt tends to zero or, equivalently, n tends to ∞.

When the POD bases $\{\psi_i\}_{i=1}^{\ell}$ and $\{\phi_i\}_{i=1}^{\ell}$ have been computed, we make the ansatz

$$u_\ell(t,\mathbf{x}) = \bar{u}(\mathbf{x}) + \sum_{j=1}^{\ell} u_\ell^j(t)\psi_j(\mathbf{x}) \quad \text{and} \quad v_\ell(t,\mathbf{x}) = \bar{v}(\mathbf{x}) + \sum_{j=1}^{\ell} v_\ell^j(t)\phi_j(\mathbf{x}) \tag{9}$$

for the POD Galerkin approximations of u and v, respectively. Recall that u_j and v_j satisfy homogeneous Dirichlet or Neumann boundary conditions on Γ. Due to Remark 2 both POD approximations u_ℓ and v_ℓ satisfy homogeneous boundary condition on Γ for the choices $(\bar{u},\bar{v}) = (u_{\text{mean}}, v_{\text{mean}})$ and $(\bar{u},\bar{v}) = (0,0)$. In this case (1b) or (1c) hold for the POD approximations u_ℓ and v_ℓ so that the boundary conditions for u_ℓ and v_ℓ are satisfied.

Inserting (9) into (1a) we find

$$\begin{aligned}\sum_{j=1}^{\ell} \dot{u}_\ell^j(t)\psi_j = \;& \lambda(s_\ell)\bar{u} - \omega(s_\ell)\bar{v} + \sigma\Delta\bar{u} + \sum_{j=1}^{\ell} u_\ell^j(t)\sigma\Delta\psi_j \\ & + \lambda(s_\ell)\sum_{j=1}^{\ell} u_\ell^j(t)\psi_j - \omega(s_\ell)\sum_{j=1}^{\ell} v_\ell^j(t)\phi_j,\end{aligned} \tag{10}$$

$$\begin{aligned}\sum_{j=1}^{\ell} \dot{v}_\ell^j(t)\phi_j = \;& \omega(s_\ell)\bar{u} + \lambda(s_\ell)\bar{v} + \sigma\Delta\bar{v} + \sum_{j=1}^{\ell} v_\ell^j(t)\sigma\Delta\phi_j \\ & + \omega(s_\ell)\sum_{j=1}^{\ell} u_\ell^j(t)\psi_j + \lambda(s_\ell)\sum_{j=1}^{\ell} v_\ell^j(t)\phi_j\end{aligned} \tag{11}$$

with $s_\ell = u_\ell(t,\cdot)^2 + v_\ell(t,\cdot)^2$ and $t \in (0,T]$. Next we multiply (10) by ψ_i, $i = 1,\ldots,\ell$, (11) by ϕ_i, $i = 1,\ldots,\ell$, and integrate over Ω. From $\int_\Omega \psi_j\psi_i\,\mathrm{d}\mathbf{x} = \int_\Omega \phi_j\phi_i\,\mathrm{d}\mathbf{x} = \delta_{ij}$ we obtain

$$\begin{pmatrix} \dot{\mathbf{u}}_\ell(t) \\ \dot{\mathbf{v}}_\ell(t) \end{pmatrix} = \sigma \begin{pmatrix} A_u\mathbf{u}_\ell(t) \\ A_v\mathbf{v}_\ell(t) \end{pmatrix} + \begin{pmatrix} F_u(\mathbf{u}_\ell(t),\mathbf{v}_\ell(t)) \\ F_v(\mathbf{u}_\ell(t),\mathbf{v}_\ell(t)) \end{pmatrix} + \begin{pmatrix} \mathbf{f}_{\bar{u}} \\ \mathbf{f}_{\bar{v}} \end{pmatrix} \quad \text{for } t \in (0,T], \tag{12a}$$

where the vectors $\mathbf{u}_\ell$, $\mathbf{v}_\ell$, $\mathbf{f}_{\bar{u}}$, $\mathbf{f}_{\bar{v}}$ satisfy

$$\mathbf{u}_\ell = \begin{pmatrix} u_\ell^1 \\ \vdots \\ u_\ell^\ell \end{pmatrix},\ \mathbf{v}_\ell = \begin{pmatrix} v_\ell^1 \\ \vdots \\ v_\ell^\ell \end{pmatrix},\ \mathbf{f}_{\bar{u}} = \begin{pmatrix} \int_\Omega \sigma\Delta\bar{u}\psi_1\,\mathrm{d}\mathbf{x} \\ \vdots \\ \int_\Omega \sigma\Delta\bar{u}\psi_\ell\,\mathrm{d}\mathbf{x} \end{pmatrix},\ \mathbf{f}_{\bar{v}} = \begin{pmatrix} \int_\Omega \sigma\Delta\bar{v}\phi_1\,\mathrm{d}\mathbf{x} \\ \vdots \\ \int_\Omega \sigma\Delta\bar{v}\phi_\ell\,\mathrm{d}\mathbf{x} \end{pmatrix},$$

the matrices A_u, A_v are given by

$$\begin{aligned} A_u &= \big((a_u^{ij})\big) \in \mathbb{R}^{\ell\times\ell} \text{ with } a_u^{ij} = \int_\Omega \Delta\psi_j\psi_i\,\mathrm{d}\mathbf{x}, \\ A_v &= \big((a_v^{ij})\big) \in \mathbb{R}^{\ell\times\ell} \text{ with } a_v^{ij} = \int_\Omega \Delta\phi_j\phi_i\,\mathrm{d}\mathbf{x}, \end{aligned}$$

and the non-linear terms

$$F_u(\mathbf{u}_\ell(t),\mathbf{v}_\ell(t)) = \begin{pmatrix} F_u^1(\mathbf{u}_\ell(t),\mathbf{v}_\ell(t)) \\ \vdots \\ F_u^\ell(\mathbf{u}_\ell(t),\mathbf{v}_\ell(t)) \end{pmatrix}, \quad F_v(\mathbf{u}_\ell(t),\mathbf{v}_\ell(t)) = \begin{pmatrix} F_v^1(\mathbf{u}_\ell(t),\mathbf{v}_\ell(t)) \\ \vdots \\ F_v^\ell(\mathbf{u}_\ell(t),\mathbf{v}_\ell(t)) \end{pmatrix}$$

are defined as

$$F_u^i(\mathbf{u}_\ell(t),\mathbf{v}_\ell(t)) = \int_\Omega \big(\lambda(s_\ell)u_\ell(t,\cdot) - \omega(s_\ell)v_\ell(t,\cdot)\big)\psi_i \,\mathrm{d}\mathbf{x},$$
$$F_v^i(\mathbf{u}_\ell(t),\mathbf{v}_\ell(t)) = \int_\Omega \big(\omega(s_\ell)u_\ell(t,\cdot) + \lambda(s_\ell)v_\ell(t,\cdot)\big)\phi_i \,\mathrm{d}\mathbf{x}$$

for $1 \le i \le \ell$. From (1d) we derive the initial condition

$$\begin{pmatrix} \mathbf{u}_\ell(0) \\ \mathbf{v}_\ell(0) \end{pmatrix} = \begin{pmatrix} \mathbf{u}_\circ \\ \mathbf{v}_\circ \end{pmatrix} - \begin{pmatrix} \bar{\mathbf{u}} \\ \bar{\mathbf{v}} \end{pmatrix} \tag{12b}$$

with

$$\mathbf{u}_\circ = \begin{pmatrix} \int_\Omega u_\circ\psi_1 \,\mathrm{d}\mathbf{x} \\ \vdots \\ \int_\Omega u_\circ\psi_\ell \,\mathrm{d}\mathbf{x} \end{pmatrix}, \qquad \mathbf{v}_\circ = \begin{pmatrix} \int_\Omega v_\circ\phi_1 \,\mathrm{d}\mathbf{x} \\ \vdots \\ \int_\Omega v_\circ\phi_\ell \,\mathrm{d}\mathbf{x} \end{pmatrix},$$
$$\bar{\mathbf{u}} = \begin{pmatrix} \int_\Omega \bar{u}\psi_1 \,\mathrm{d}\mathbf{x} \\ \vdots \\ \int_\Omega \bar{u}\psi_\ell \,\mathrm{d}\mathbf{x} \end{pmatrix}, \qquad \bar{\mathbf{v}} = \begin{pmatrix} \int_\Omega \bar{v}\phi_1 \,\mathrm{d}\mathbf{x} \\ \vdots \\ \int_\Omega \bar{v}\phi_\ell \,\mathrm{d}\mathbf{x} \end{pmatrix}.$$

Summarizing the POD reduced-order model is given by (12) that is solved numerically in Section 4 for different values for the parameter β in (2) and number ℓ of POD ansatz functions.

4 NUMERICAL EXPERIMENTS

This section is devoted to present two numerical test examples. All coding is done in MATLAB. The programs are executed on a standard Pentium D, 3 Ghz desktop PC.

We choose the initial conditions

$$u_\circ(x,y) = y - \frac{1}{2} \quad \text{and} \quad v_\circ(x,y) = \frac{x}{2} - \frac{1}{4}.$$

The snapshots $\{(u_j, v_j)\}_{j=1}^n$ are computed by applying a finite difference approximation for the spatial domain (with a five-point discretization for the Laplace operator). In (4) we choose $T = 50$, $n = 501$ and the spatial equidistant mesh size $h > 0$ and the corresponding grid points $\mathbf{x}_{ij} = (x_i, y_j) \in \overline{\Omega}$ are given by

$$h = \frac{1}{N+1}, \quad x_i = ih \text{ for } 0 \le i \le N+1, \quad y_j = jh \text{ for } 0 \le j \le N+1.$$

After spatial discretization we arrive at an initial-value problem for $2N^2$ coupled ordinary differential equations in case of boundary condition (1b) and for $2(N+2)^2$ coupled ordinary differential equations in case of (1c). These systems are solved by the MATLAB routine `ode15s` to obtain an approximation (u_h, v_h) to the solution of (1). As snapshots we take the ensemble $\{(u_h(t_j,\cdot), v_h(t_j,\cdot))\}_{j=1}^{501}$.

4.1 Dirichlet boundary conditions

Let us investigate the λ-ω system with homogeneous Dirichlet boundary conditions. We analyze numerically the dependence of the accuracy of the reduced-order model on the parameter β in (2). First we compute the $n = 501$ snapshots, solve the eigenvalue problems (7), (8) and determine the POD bases $\{\psi_i\}_{i=1}^{\ell}$ and $\{\chi_i\}_{i=1}^{\ell}$. The routine `ode15s` needs 2644.09 seconds and the computation of the reduced-order model requires about 4.5 seconds for $\ell = 50$. The decay of the first 50 eigenvalues is shown in Figure 3. We

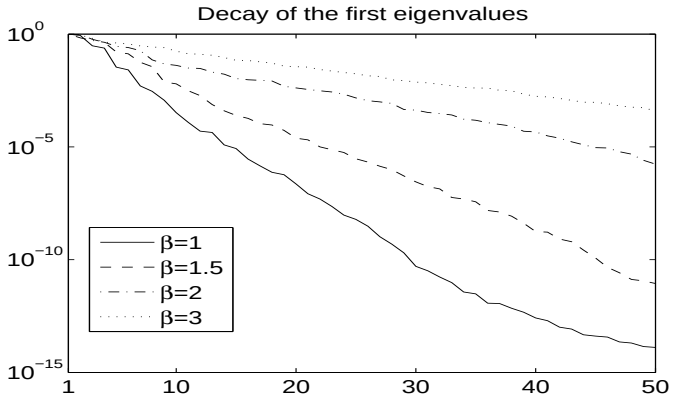

Figure 3: Decay of the first eigenvalues for different values of β in (1) and homogeneous Dirichlet boundary conditions.

observe from Figure 3 that the eigenvalues decay slower for increasing parameter β. For small β only a few modes are needed to reflect the evolution of the whole system, but with increasing β the model becomes turbulent. Therefore, the eigenvalues decay not as fast as for smaller parameter β.

Next we take $\bar{u} = \bar{v} = 0$ (no offsets in the POD Galerkin projection) and solve the reduced-order model by applying the MATLAB solver `ode15s`. In Figure 4 we compare the relative errors

$$t \mapsto \frac{\|u_\ell(t) - u_h(t)\|^2}{\|u_h(t)\|^2}$$

for $\beta = 1.5$ (left plot) and $\beta = 2$ (right plot). It turns out that for $\beta = 1.5$ (left plot in Figure 4) even $\ell = 10$ POD ansatz functions are sufficient to obtain a reliable reduced-order model. On the other hand, for $\beta = 2$ the POD solution based on $\ell = 10$ is completly

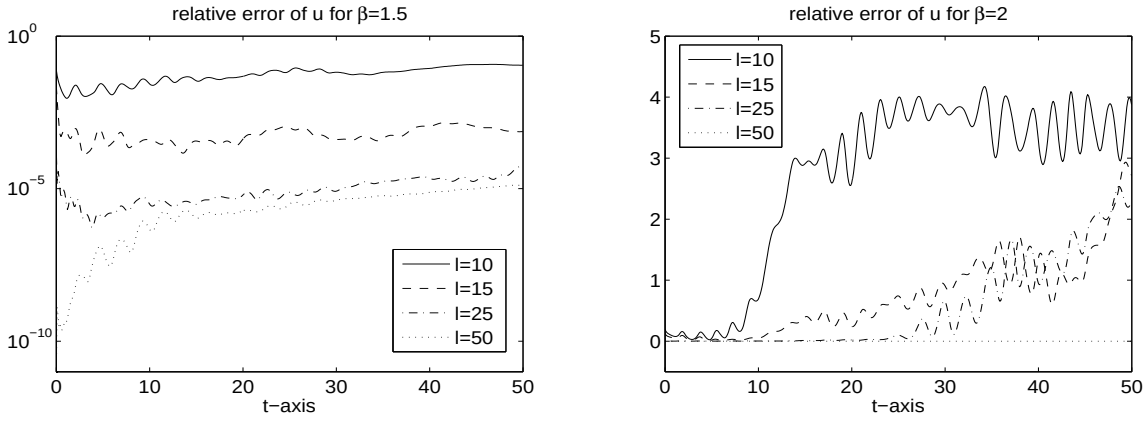

Figure 4: Relative errors for $\beta = 1.5$ (left plot) and $\beta = 2$ (right plot) in case of homogeneous Dirichlet boundary conditions and $\ell = 10$, 15, 25, 50.

different from the finite difference solution. Also for $\ell = 15$ and $\ell = 25$ we observe that the relative errors increase drastically for $t > 25$ and $t > 30$, respectively. Using $\ell = 50$ POD basis functions yields a reliable POD solution that is close to the finite difference solution u^h. In Table 1 the relative errors

$$E_{\mathrm{rel}}(u) = \frac{\sum_{j=1}^{n} \alpha_j \left\| u_\ell(t_j) - u_h(t_j) \right\|^2}{\sum_{j=1}^{n} \alpha_j \left\| u_h(t_j) \right\|^2}$$

are presented. We observe that the errors decrease if ℓ increase. Moreover, for larger

ℓ	$\beta = 1$	$\beta = 1.5$	$\beta = 2$	$\beta = 2.5$	$\beta = 3$
10	0.0002742	0.0592466	2.6147003	2.0664552	1.9121706
15	0.0000399	0.0006219	0.7012245	1.6072066	2.0462711
25	0.0000003	0.0000108	0.5548754	1.5939146	1.5950328
50	0.0000001	0.0000039	0.0000519	0.2994985	0.9057551

Table 1: The relative error $E_{\mathrm{rel}}(u)$ for different numbers ℓ of POD ansatz functions and for different values of the parameter β in (1) in case of homogeneous Dirichlet boundary conditions.

values of β the errors increases for fixed number ℓ of POD ansatz functions. In particular, for $\beta = 3$ the error for $\ell = 50$ is quite high so that we should include more POD basis functions in our reduced-order approach. The relative errors $E_{\mathrm{rel}}(v)$ for the v are plotted in Table 2. The results for the POD solution v_ℓ are similar than the results for u_ℓ.

4.2 Neumann boundary conditions

Now we consider the λ-ω system with the homogeneous Neumann boundary conditions (1c). It turns out that the dependence of the quality of the reduced-order model depends

ℓ	$\beta = 1$	$\beta = 1.5$	$\beta = 2$	$\beta = 2.5$	$\beta = 3$
10	0.0002699	0.0588345	2.6087718	2.0671781	1.9116376
15	0.0000038	0.0006968	0.6998566	1.5974137	2.0528978
25	0.0000026	0.0000105	0.5590867	1.5945250	1.5956316
50	0.0000001	0.0000039	0.0000512	0.2970237	0.9108994

Table 2: The relative error $E_{\text{rel}}(v)$ for different numbers ℓ of POD ansatz functions and for different values of the parameter β in (1) in case of homogeneous Dirichlet boundary conditions.

on the size of the parameter β. The computation of the reduced-order model for (1) is done analogously as described in Section 4.1. The CPU time to compute the $n = 501$ snapshots is 3176.03 seconds and the calculation of the POD bases requires about 4.5 seconds for $\ell = 50$ ansatz functions. The decay of the first 50 eigenvalues is shown in Figure 5. Thus,

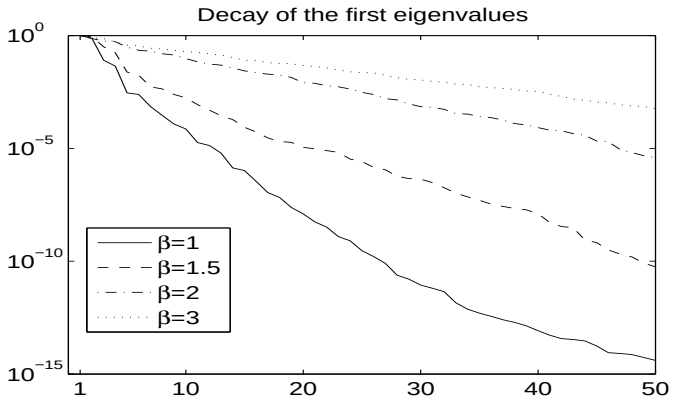

Figure 5: Decay of the first eigenvalues for different values of β in (1) and homogeneous Neumann boundary conditions.

the decay rate of the eigenvalues has the same dependence on the parameter β as in the case of homogeneous Dirichlet boundary conditions.

Let us compare the quality of the reduced-order solution with respect to the choice of the offset $\bar{u}$ and $\bar{v}$ in the POD Galerkin projection (compare Remark 2). In Table 3 we plot the relative errors $E_{\text{rel}}(u)$ and the CPU times for the solution of the reduced-order model (12) for $\beta = 1.5$. We observe that there is no big difference in the errors. Thus, for small values of β we can take $\bar{u} = 0$ to get a reliable reduced-order model. between the two methods. Note that the POD solve is — depending on ℓ — much faster than the finite difference solve. In Table 4 we compare the errors for the two different offsets in case of $\beta = 2$, where the λ-ω systems has already turbulent features. For $\beta = 2$ with $\ell < 40$ we get no usefull results, so we compare the errors for the choice $\ell = 40$, 45, 50. We observe that the POD model reduction performs better provided we take $\bar{u} = u_{\text{mean}}$. Note that for $\bar{u} = 0$ the POD solutions differ significantly from the finite difference solution in case of $\ell = 40$ and 45.

	$\bar{u} = 0$	$\bar{u} = u_{\text{mean}}$	CPU-time
$\ell = 10$	0.0058895	0.0059449	17.0 seconds
$\ell = 15$	0.0003499	0.0003351	35.9 seconds
$\ell = 25$	0.0000305	0.0000257	54.3 seconds
$\ell = 50$	0.0000093	0.0000092	139.2 seconds

Table 3: The relative error $E_{\text{rel}}(u)$ for different numbers ℓ of POD ansatz functions and for different types of POD calculation and for $\beta = 1.5$ in (2) in case of homogeneous Neumann boundary conditions (1b) and the CPU times.

	$\bar{u} = 0$	$\bar{u} = u_{\text{mean}}$
$\ell = 40$	0.5774415	0.4601877
$\ell = 45$	0.8986130	0.2976193
$\ell = 50$	0.0710348	0.0017736

Table 4: The relative error $E_{\text{rel}}(u)$ for different numbers ℓ of POD ansatz functions and for different types of POD calculation for $\beta = 2$ in (2) in case of homogeneous Neumann boundary conditions.

4.3 Predictor corrector method

From the numerical experiments carried out in Sections 4.1 and 4.2 we observe that for $\beta \geq 2$ the number of POD basis functions used for the model reduction should be larger than 25. On the other hand, the more POD ansatz functions in the POD are used, the more time is needed by the POD solver of the λ-ω system. Since the most energy is contained in the lower modes, we split the ansatz for u and v as follows:

$$u_\ell(t,\mathbf{x}) = \bar{u}(\mathbf{x}) + \sum_{j=1}^{\ell_1} u_\ell^j(t)\psi_j(\mathbf{x}) + \sum_{j=\ell_1+1}^{\ell} u_\ell^j(t)\psi_j(\mathbf{x}) = \bar{u}(\mathbf{x}) + u_{\text{low}}(t,\mathbf{x}) + u_{\text{high}}(t,\mathbf{x}),$$
$$v_\ell(t,\mathbf{x}) = \bar{v}(\mathbf{x}) + \sum_{j=1}^{\ell_1} v_\ell^j(t)\phi_j(\mathbf{x}) + \sum_{j=\ell_1+1}^{\ell} v_\ell^j(t)\phi_j(\mathbf{x}) = \bar{v}(\mathbf{x}) + v_{\text{low}}(t,\mathbf{x}) + v_{\text{high}}(t,\mathbf{x}),$$

where

$$u_{\text{low}}(t,\mathbf{x}) = \sum_{j=1}^{\ell_1} u_\ell^j(t)\psi_j(\mathbf{x}), \qquad u_{\text{high}}(t,\mathbf{x}) = \sum_{j=\ell_1+1}^{\ell} u_\ell^j(t)\psi_j(\mathbf{x}),$$
$$v_{\text{low}}(t,\mathbf{x}) = \sum_{j=1}^{\ell_1} v_\ell^j(t)\phi_j(\mathbf{x}), \qquad v_{\text{high}}(t,\mathbf{x}) = \sum_{j=\ell_1+1}^{\ell} v_\ell^j(t)\phi_j(\mathbf{x}).$$

Algorithm 2 (Predictor-Corrector method)

0) *Let* $\ell = \ell_1 + \ell_2$, $\Delta\tau \in (0, T]$; *put* $k = 1$.

1) *Set*

$$u_{\text{high}}^k = \sum_{j=\ell_1+1}^{\ell} \langle u_\circ, \psi_j \rangle \, \psi_j(\mathbf{x}), \qquad v_{\text{high}}^k = \sum_{j=\ell_1+1}^{\ell} \langle v_\circ, \phi_j \rangle \, \phi_j(\mathbf{x}),$$

$$\mathbf{u}_{\text{high}}^k = \begin{pmatrix} \langle u_{\text{high}}^k, \psi_{\ell_1+1} \rangle \\ \vdots \\ \langle u_{\text{high}}^k, \psi_\ell \rangle \end{pmatrix}, \qquad \mathbf{v}_{\text{high}}^k = \begin{pmatrix} \langle v_{\text{high}}^k, \phi_{\ell_1+1} \rangle \\ \vdots \\ \langle v_{\text{high}}^k, \phi_\ell \rangle \end{pmatrix}$$

and solve the ℓ_1-dimensional problem

$$\begin{pmatrix} \dot{\mathbf{u}}_{\ell_1}(t) \\ \dot{\mathbf{v}}_{\ell_1}(t) \end{pmatrix} = \sigma \begin{pmatrix} A_u \mathbf{u}_{\ell_1}(t) \\ A_v \mathbf{v}_{\ell_1}(t) \end{pmatrix} + \begin{pmatrix} F_u^k(\mathbf{u}_{\ell_1}(t), \mathbf{v}_{\ell_1}(t)) \\ F_v^k(\mathbf{u}_{\ell_1}(t), \mathbf{v}_{\ell_1}(t)) \end{pmatrix} + \begin{pmatrix} \mathbf{f}_{\bar{u}} \\ \mathbf{f}_{\bar{v}} \end{pmatrix}$$

on the interval $\big[(k-1)\Delta\tau, k\Delta\tau\big] = [0, \Delta\tau]$, where

$$(F_u^k)^i(\mathbf{u}_{\ell_1}(t), \mathbf{v}_{\ell_1}(t)) = \int_\Omega \Big(\lambda(s_\ell)\big(u_{\ell_1}(t,\cdot) + u_{\text{high}}^k\big) - \omega(s_\ell)\big(v_{\ell_1}(t,\cdot) + v_{\text{high}}^k\big)\Big)\psi_i \, \mathrm{d}\mathbf{x},$$

$$(F_v^k)^i(\mathbf{u}_{\ell_1}(t), \mathbf{v}_{\ell_1}(t)) = \int_\Omega \Big(\omega(s_\ell)\big(u_{\ell_1}(t,\cdot) + u_{\text{high}}^k\big) + \lambda(s_\ell)\big(v_{\ell_1}(t,\cdot) + v_{\text{high}}^k\big)\Big)\phi_i \, \mathrm{d}\mathbf{x}$$

for $i = 1, \ldots, \ell_1$ by the explicit Euler method.

2) *Compute $(\mathbf{u}_{\text{high}}^{k+1}, \mathbf{v}_{\text{high}}^{k+1}) \in \mathbb{R}^{\ell_2} \times \mathbb{R}^{\ell_2}$ from*

$$\frac{1}{\Delta\tau} \begin{pmatrix} \mathbf{u}_{\text{high}}^{k+1} - \mathbf{u}_{\text{high}}^k \\ \mathbf{v}_{\text{high}}^{k+1} - \mathbf{v}_{\text{high}}^k \end{pmatrix} = \sigma \begin{pmatrix} A_u \mathbf{u}_{\text{high}}^k \\ A_v \mathbf{v}_{\text{high}}^k \end{pmatrix} + \begin{pmatrix} F_u^k(\mathbf{u}_{\ell_1}(t), \mathbf{v}_{\ell_1}(t)) \\ F_v^k(\mathbf{u}_{\ell_1}(t), \mathbf{v}_{\ell_1}(t)) \end{pmatrix} + \begin{pmatrix} \mathbf{f}_{\bar{u},\text{high}} \\ \mathbf{f}_{\bar{v},\text{high}} \end{pmatrix}.$$

Set $k = k+1$ and define

$$u_{\text{high}}^k = \sum_{j=\ell_1+1}^{\ell} \big(\mathbf{u}_{\text{high}}^k\big)^j \, \psi_j(\mathbf{x}), \quad v_{\text{high}}^k = \sum_{j=\ell_1+1}^{\ell} \big(\mathbf{v}_{\text{high}}^k\big)^j \, \phi_j(\mathbf{x}).$$

3) *Solve the ℓ_1-dimensional problem*

$$\begin{pmatrix} \dot{\mathbf{u}}_{\ell_1}(t) \\ \dot{\mathbf{v}}_{\ell_1}(t) \end{pmatrix} = \sigma \begin{pmatrix} A_u \mathbf{u}_{\ell_1}(t) \\ A_v \mathbf{v}_{\ell_1}(t) \end{pmatrix} + \begin{pmatrix} F_u^k(\mathbf{u}_{\ell_1}(t), \mathbf{v}_{\ell_1}(t)) \\ F_v^k(\mathbf{u}_{\ell_1}(t), \mathbf{v}_{\ell_1}(t)) \end{pmatrix} + \begin{pmatrix} \mathbf{f}_{\bar{u}} \\ \mathbf{f}_{\bar{v}} \end{pmatrix}$$

on the interval $\big[(k-1)\Delta\tau, k\Delta\tau\big] = [\Delta\tau, 2\Delta\tau]$.

4) *Go back to step 2) unless the terminal time T is reached.*

Note that we use the first ℓ_1 POD basis functions for the (linear) POD Galerkin approximation and utilize the estimates $(\mathbf{u}_{\text{high}}^k, \mathbf{v}_{\text{high}}^k)$ as an approximation for the higher $(j > \ell_1)$ POD modes. This estimates are taken to correct the estimated POD solutions $(\mathbf{u}_{\ell_1}, \mathbf{v}_{\ell_1})$.

Let $\delta t = 0.001$ be the time step for the explicit method and $\Delta\tau = l\delta t$. First we compare the predictor-corrector method to the linear Galerkin algorithm for $\beta = 2$ and homogeneou Neumann boundary conditions on the time interval $[0, 40]$. For every combination of ℓ_1 and ℓ_2 two runs with $l = 10$ and $l = 100$ are made. Because of the turbulent behavior of the system $t > 20$, we take the same large values of ℓ as in Table 4 and also the mean $\bar{u} = u_{\text{mean}}$ is used in both methods. The Galerkin method with $\ell = 50$ has the lowest relative error,

Solve of (12)		Algorithm 2		
			$l = 10$	$l = 100$
$\ell = 40$	0.22277	$\ell_1 = 20$, $\ell_2 = 30$	0.13152	1.27117
$\ell = 45$	0.04672	$\ell_1 = 25$, $\ell_2 = 25$	0.02288	0.96374
$\ell = 50$	0.00036	$\ell_1 = 30$, $\ell_2 = 20$	0.00624	0.02526

Table 5: Comparison of the relative error $E_{\text{rel}}(u)$ between the solution of (12) for fixed ℓ on $[0, T]$ and the predictor corrector method for $T = 40$, $\beta = 2$ and homogeneous Neumann boundary conditions.

because all modes are updated in every step. Choosing $l = 100$ the predictor-corrector method with ℓ_1 lower than 30 results in a large relative error, for $\ell_1 = 30$ the results are slightly better than the solution of (12) in case of $\ell = 45$. Reducing l to 10 really improves the predictor-corrector method, because the higher modes are updated more often.

In a second test with the same β, but only on the time interval $[0, 20]$ we compare the methods for a smaller number of modes. Now for the smaller l the relative error of the

Solve of (12)		Algorithm 2		
			$l = 10$	$l = 100$
$\ell = 15$	0.47865	$\ell_1 = 10$, $\ell_2 = 15$	0.08831	0.56038
$\ell = 25$	0.09955	$\ell_1 = 15$, $\ell_2 = 10$	0.09243	0.11447

Table 6: Comparison of the relative error $E_{\text{rel}}(u)$ between the solution of (12) for fixed ℓ on $[0, T]$ and the predictor-corrector method for $T = 20$, $\beta = 2$ and homogeneous Neumann boundary conditions.

predictor-corrector approach is even a little smaller than for the Galerkin with $\ell = \ell_1 + \ell_2$, but this has no significance. The Galerkin method with $\ell = 15$ is much worse than the predictor-corrector method. After setting $l = 100$ the number of lower modes has to be increased to 15, otherwise the error is to large.

When the cost for the solution of the reduced system depends strongly on the number of modes, then the proposed predictor-corrector method gives the chance to get accurate results in a shorter time, because the higher modes are not updated that often.

4.4 Snapshot archetypes by Adrover

If the calculation of the POD basis from all snapshots is very time-consuming, then it is usefull to reduce the number of snapshots. On one hand, this could be done by increasing the time differences Δt between the snapshots, on the other hand a selection rule like the one proposed in [1] can be applied.

Algorithm 1 (Choice of snapshots [1])

0) *Fix the number* $\bar{k} \in \{2, \ldots, n\}$ *of snapshots.*

1) *Set* $\tilde{u}_1 = u_\circ$, $t_{i_1} = t_1 = 0$ *and* $k = 1$.

2) *Determine*

$$t_{k+1} = \operatorname{argmax} \left\{ \min_{1 \le l \le k} \left\| u(t_j, \cdot) - u(t_{i_l}, \cdot) \right\| \,\middle|\, t_j \in \{t_1, \ldots, t_n\} \setminus \{t_{i_1}, \ldots, t_{i_k}\} \right\}$$

3) *Set* $k = k + 1$ *and* $\tilde{u}_k(\mathbf{x}) = u(t_k, \mathbf{x})$ *for all* $\mathbf{x} \in \Omega$. *If* $k < \bar{k}$, *go back to step* 2).

We choose the parameter $\beta = 1.5$, the terminal time $T = 50$ and homogeneous Neumann boundary conditions (1c). The goal is to perform the POD reduced-order modeling by taking only $\bar{k} = 100$ instead of $n = 501$ snapshots. We compute the snapshots $\{\tilde{u}_j\}_{j=1}^{100}$ by Algorithm 1 with the ensemble $\{\bar{u}_j\}_{j=1}^{100}$ with $\bar{u}_j = u((j-1)5\Delta t, \cdot)$ (i.e., compared to (4) we take a 5 times coarser grid). In Table 7 we compare the relative error $E_{\mathrm{rel}}(u)$ for different numbers ℓ of POD ansatz functions, where the POD basis is determined by utilizing the snapshots $\{\bar{u}_j\}$ (coarse time grid), $\{\tilde{u}_j\}_{j=1}^{100}$ (Algorithm 1) and $\{\hat{u}_j\}_{j=1}^{501}$ (fine time grid). Let us mention that we take zero offsets in (9). We observe that the results

	coarse time grid	Algorithm 1	fine time grid
$\ell = 10$	0.0059044	0.0087575	0.0058895
$\ell = 15$	0.0003583	0.0005443	0.0003499
$\ell = 25$	0.0000285	0.0000541	0.0000305
$\ell = 50$	0.0000081	0.0000127	0.0000093

Table 7: The relative error $E_{\mathrm{rel}}(u)$ for different numbers ℓ of POD ansatz functions and $\beta = 1.5$, where the POD was calculated on a coarse time grid, by the preselection rule (Algorithm 1) or on the fine time grid (4).

for the coarse time grid are as good as the corresponding ones for the fine time grid, but the errors for the POD Galerkin solution computed via the snapshots determined by Algorithm 1 are higher.

5 CONCLUSIONS

In this article reduced-order approximations for λ-ω systems are considered by applying POD Galerkin projection. It turns out that the quality of the POD Galerkin approximation depends on a parameter β in the λ-Ω system. The higher the parameter β is chosen the more turbulent behavior the solution has. Numerical experiments for the Dirichlet- and Neumann boundary conditions are presented. We compare the linear Galerkin scheme with a predictor-corrector method. Motivated by our observations the extension of our predictor-corrector method to non-linear Galerkin approximations can be a focus of future research.

REFERENCES

[1] A. Adrover and M. Giona. Modal reduction of PDE models by means of snapshot archetypes. *Physica D*, **182**, 23–45 (2003).

[2] J.A. Atwell and B.B. King. Reduced order controllers for spatially distributed systems via proper orthogonal decomposition. *SIAM Journal on Scientific Computing*, **26**, 128–151 (2004).

[3] H.T. Banks, M.L. Joyner, B. Winchesky, and W.P. Winfree. Nondestructive evaluation using a reduced-order computational methodology. *Inverse Problems*, **16**, 1–17, (2000).

[4] H.T. Banks, R.C.H. del Rosario, and R.C. Smith. Reduced order model feedback control design: numerical implementation in a thin shell model. Technical Report CRSC-TR98-27, North Carolina State University, (1998).

[5] A. Borzì and R. Griesse. Distributed optimal control of lambda-omega systems. *Journal of Numerical Mathematics*, to appear, (2006).

[6] A. Borzì and R. Griesse. Experiences with a space-time multigrid method for the optimal control of a chemical turbulence model. *International Journal for Numerical Methods in Fluids*, **47**, 879–885 (2005).

[7] M. Cross and P. Hohenberg. Pattern formation outside of equilibrium. *Reviews of Modern Physics*, **65**, 851–1112, (1993).

[8] E.D. Dahlberg and J.G. Zhu. Micromagnetic microscopy and modeling. *Physics Today*, **48**, p. 34 (1995).

[9] M. Fahl. Computation of POD basis functions for fluid flows with Lanczos methods. *Mathematical and Computer Modelling*, **34**, 91–107, (2001).

[10] K. Fukuda. *Introduction to Statistical Recognition*. Academic Press, New York, (1990).

[11] M. Hinze and S. Volkwein. Error estimates for abstract linear-quadratic optimal control problems using proper orthogonal decomposition. Technical Report No. IMA02-05, Institute of Mathematics and Scientific Computing, University of Graz, submitted, (2005).
See `http://www.uni-graz.at/imawww/reports/archive-2005/IMA02-05.pdf`.

[12] P. Holmes, J.L. Lumley, and G. Berkooz. *Turbulence, Coherent Structures, Dynamical Systems and Symmetry*. Cambridge Monographs on Mechanics, Cambridge University Press, (1996).

[13] C. Homescu, L.R. Petzold, and R. Serban. Error estimation for reduced order models of dynamical systems. *SIAM Journal on Numerical Analysis*, **43**, 1693–1714, (2005).

[14] M. Kahlbacher and S. Volkwein. Galerkin proper orthogonal decomposition methods for parameter dependent elliptic systems. Technical Report No. IMA06-06, Institute of Mathematics and Scientific Computing, University of Graz, submitted, (2006).
See `http://www.uni-graz.at/imawww/reports/archive-2006/IMA06-06.pdf`.

[15] M. Kahlbacher and S. Volkwein. Model reduction by proper orthogonal decomposition for estimation of scalar parameters in elliptic PDEs. Technical Report No. IMA14-06, Institute of Mathematics and Scientific Computing, University of Graz, submitted, (2006).
See `http://www.uni-graz.at/imawww/reports/archive-2006/IMA14-06.pdf`.

[16] K. Kunisch and S. Volkwein. Galerkin proper orthogonal decomposition methods for parabolic problems. *Numerische Mathematik*, **90**, 117–148, (2001).

[17] K. Kunisch and S. Volkwein. Galerkin proper orthogonal decomposition methods for a general equation in fluid dynamics. *SIAM Journal on Numerical Analysis*, **40**, 492–515, (2002).

[18] K. Kunisch and S. Volkwein. Proper orthogonal decomposition for optimality systems. Technical Report No. IMA10-06, Institute of Mathematics and Scientific Computing, University of Graz, submitted, (2006).
See `http://www.uni-graz.at/imawww/reports/archive-2006/IMA10-06.pdf`.

[19] Y. Kuramoto. *Chemical Oscilliations, Waves and Turbulence*. Springer-Verlag, Berlin, (1984).

[20] Y. Kuramoto and S. Koga. Turbulized rotating chemical waves. *Prog. Theor. Phys.*, **66**, 1081–1085, (1981).

[21] S. Lall, J.E. Marsden and S. Glavaski. Empirical model reduction of controlled nonlinear systems. In: *Proceedings of the IFAC Congress*, **vol. F**, 473–478, (1999).

[22] H.V. Ly and H.T. Tran. Modelling and control of physical processes using proper orthogonal decomposition. *Mathematical and Computer Modeling*, **33**, 223–236, (2001).

[23] P. Manneville. *Dissipative Structures and Weak Turbulence*. Academic Press, Boston, (1990).

[24] J.D. Murray. *Mathematical Biology*. Springer-Verlag, Berlin, (1993).

[25] M. Rathinam and L. Petzold. Dynamic iteration using reduced order models: a method for simulation of large scale modular systems. *SIAM Journal on Numerical Analysis*, **40**, 1446–1474, (2002).

[26] C. W. Rowley. Model reduction for fluids, using balanced proper orthogonal decomposition. *International Journal of Bifurcation and Chaos*, **15**, 997–1013, (2005).

[27] J.A. Sherratt. On the evolution of periodic plane waves in reaction-diffusion systems of λ-ω type. *SIAM Journal on Applied Mathematics*, **54**, 1374–1385, (1954)

[28] L. Sirovich. Turbulence and the dynamics of coherent structures, parts I-III. *Quarterly of Applied Mathematics*, **XLV**, 561–590, (1987).

[29] R. Temam. *Infinite-dimensional Dynamical Systems in Mechanics and Physics*. Springer-Verlag, New York, (1994).

[30] S. Volkwein. Optimal control of a phase-field model using the proper orthogonal decomposition. *Zeitschrift für Angewandte Mathematik und Mechanik*, **81**, 83–97, (2001).

[31] K. Willcox and J. Peraire. Balanced model reduction via the proper orthogonal decomposition. *American Institute of Aeronautics and Astronautics (AIAA)*, 2001–2611, (2001).